Fabrication of clamped-clamped beam resonators with embedded fluidic nanochannel

Fabrication of clamped-clamped beam resonators with embedded fluidic nanochannel

Davide Scaiola[a, b], Stefano Stassi[a], Roberta Calmo[a], Damien Maillard[c], Stefano S. G. Varricchio[b], Annalisa De Pastina[c], Guillermo Villanueva[c], Philippe Renaud[b], Carlo Ricciardi[a,*]

[a] Dipartimento di Scienza Applicata e Tecnologia, Politecnico di Torino, Torino, 10129, Italy
[b] EPFL-STI-IMT-LMIS4, École polytechnique fédérale de Lausanne, Lausanne, 1015, Switzerland
[c] EPFL-STI-IGM-NEMS, École polytechnique fédérale de Lausanne, Lausanne, 1015, Switzerland

*carlo.ricciardi@polito.it

Abstract:
Suspended nanochannel resonators (SNRs) are promising devices able to characterize mass down to the attogram scale, thus being able to detect nanoparticles or biomolecules. In this paper, we present a flexible fabrication process for SNRs based on a sacrificial layer approach that allows to easily tailor the dimensions of the nanochannel by changing the thickness of the sacrificial layer or its patterning during the lithographic step. The resonance properties of the fabricated SNR are investigated in terms of resonance frequency and frequency stability (Allan deviation). Liquids of different densities are injected in the device and, from the shift of the resonance peaks, the mass responsivity of the resonators is assessed to be up to 3.90 mHz/ag. To the best of our knowledge, the devices here presented are the first example of suspended nanochannel resonators with a channel height as low as 50 nm fabricated with a top-down approach.

Keywords: suspended nanochannel resonator, nanofabrication, mass sensor, NEMS

1. Introduction

In the last decades, micro- and nano-mechanical resonators, such as cantilevers or clamped-clamped beams, have been exploited as mass sensors in many fields [1]. In particular, a growing attention has been given to life science applications like biomedical analysis and biochemical detection [2-5]. Resonator fabrication processes usually require the same techniques of standard semiconductor technology that allow mass production and CMOS integration, and recently even 3D printing techniques started to be used [6-9]. In this way the functionalization used in biological essays is directly encapsulated in the polymer used as structural material, thus making faster and easier their usage [6]. The main limitation to the use of nanomechanical resonators for biological or biochemical assays is the loss of sensitivity due to viscous damping when vibrating in the liquid solutions, the natural environment of biological analytes. Burg *et al.* in 2007 bypassed the problem embedding a microfluidic channel in a cantilever operating in vacuum, thus constraining the liquid inside the device and almost suppressing the viscous damping [10]. They demonstrated that the quality factor of the resonator, and thus the minimum mass sensitivity achievable by the sensor, was not affected by the presence of the liquid inside the channel [11]. This finding opened the way to a new family of devices named suspended microchannel resonator (SMR) [12]. The real-time measurement in liquid environment with high mass responsivity promoted their application as chemical and biological detectors for bacteria, cells populations, and other micron-sized analytes [10, 13-15]. Suspended nanochannel resonators (SNR) with reduced mass and dimensions compared to SMR were then introduced to further improve resolution and increase device sensitivity. The miniaturization process allowed to characterize nanoparticles, where few successful attempts demonstrated that the mass sensitivity has been increased up to the attogram scale [16, 17].

The challenging fabrication remains the main bottleneck of both SMR and SNR devices. Previously reported fabrication processes are based on the sacrificial layer approach [10, 18, 19], silicon self-assembling [20] or laser etching of monolithic glass [21]. Scaling the sacrificial layer approach, based on wet etching, to the nanoscale is hard to implement, since it would take several hours to empty the channel. On the other hand, the geometry of the nanometric features of the device is hard to be fine controlled with the other two techniques.

In this paper, we present a wafer-scale fabrication process based on sacrificial layer approach with releasing of the channel done with a xenon difluoride (XeF_2) based dry etching. The dry etching approach allows a fast removal of the dummy material with respect to the previously described wet etching approach. The vertical dimension (height) of the channel is defined by the thickness of the sacrificial layer, while the horizontal dimensions (length and width) are patterned through photo-lithographic steps, so that all the dimensions can be easily adjusted to the application needs and precisely tuned. A process yield around 50% was achieved for microbeams that are 50 μm long, 7μm width and 450 nm thick, with embedded nano-channels that are 50 nm high and 3 μm width. The mechanical response of the devices is accurately characterized and their use as density/mass sensor is proven thanks to a mass responsivity up to 3.90 ± 0.72 mHz/ag and an estimated minimum detectable mass up to 595 ag. The fabricated devices represent the first examples of suspended nanochannel resonators with thickness of the embedded nanochannel below one hundred nanometers, paving the way to single nanoparticle detection in liquid.

2. Materials and methods

2.1 Design of the resonators

The design of a mechanical resonator is realized taking into account the theoretical mass responsivity of the sensor. It corresponds to the variation of resonance frequency due to a change in its mass[22]:

$$R = \frac{\partial f}{\partial m} = -\frac{1}{2}\frac{f_0}{m} \qquad (1)$$

where f_0 and m are the SNR resonance frequency and mass, respectively. In order to maximize the mass responsivity, a beam should thus have both high resonance frequency and small mass. The clamped-clamped beams presented in this work are 50 μm long, 7μm width and 450 nm thick. The embedded nano-channels are 50 nm high and 2 μm narrower than the beam width (thus 3 μm). These dimensions have been chosen in the perspective of detecting silver nanoparticles of 30 nm diameter flowing in the channel, considering a theoretical mass responsivity of R = 3.26 mHz/ag (considering a slight tensile stress induced by the anodic bonding) [22, 23].

2.2 Materials and Fabrication

The process flow developed in this work, based on the sacrificial layer approach, is sketched in Figure 1. For the fabrication of the suspended nanochannel resonator, silicon oxide deposited by low-pressure chemical-vapor-deposition (LPCVD) using TEOS (tetraethyl orthosilicate) as precursor was used as beam structural layer, while monocrystalline silicon as bulk material and sputtered polycrystalline silicon as sacrificial layer. Polycrystalline silicon has been chosen to use xenon difluoride (XeF_2) as dry etching agent for the releasing step of the sacrificial layer, since its high selectivity to SiO_2 (over 1:1000) [24]. Such high selectivity is necessary since the nanochannel

geometry requires long releasing times of about one hour. A lower etching selectivity would damage the SiO_2 structure causing also the removal of bulk silicon. Furthermore, the dry etching has been preferred to the wet one to avoid stiction during the channel releasing step. TEOS LPCVD was chosen for the deposition of SiO_2 over plasma enhanced CVD (PECVD) sputtering and low thermal oxide (LTO), because it did not show delamination problems as happened with oxides deposited with the other techniques. Moreover, the high conformality of LPCVD TEOS process fully covers the sacrificial layer even on the vertical edges, giving a smooth surface needed to encapsulate the SNR with anodic bonding. Furthermore, the layer is deposited and annealed at 710°C, to obtain a slight residual tensile stress in the film to avoid buckling problem [25].

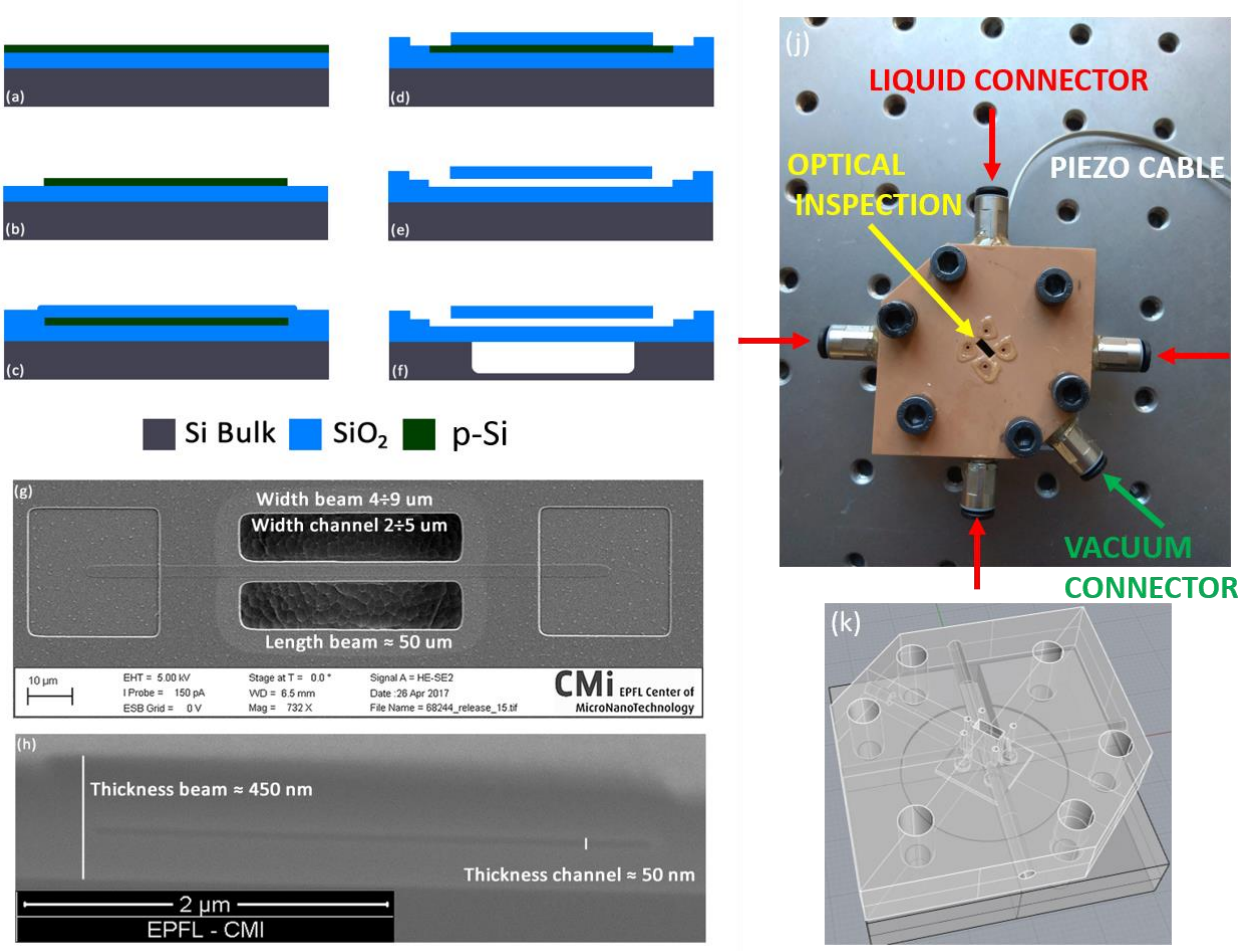

Figure 1: SNR fabrication process in cross section. a) 200 nm of TEOS LPCVD SiO_2 and 50 nm of polycrystalline Silicon (p-Si) are deposited. b) The p-Si is patterned in lines 3 µm wide and 120 µm long to define the nanochannel geometry. c) 200 nm of TEOS LPCVD SiO_2 is deposited to encapsulate the p-Si sacrificial layer. d) Two openings are etched to allow access to sacrificial layer. e) Sacrificial layer is etched with XeF_2. f) Beams are defined and released with XeF_2. g) SEM picture of a released clamped-clamped beam. h) Cross section obtained with a FIB cut in the middle of a bridge showing the polycrystalline silicon sacrificial layer surrounded by silicon oxide (darker layer). j) Image of the chip connector with the description of the different connections. k) Schematic of the chip connector showing the channels inside the 3D printed connector part.

The fabrication process starts with a deposition of 200 nm thick SiO_2 layer (LPCVD TEOS) and 50 nm of sputtered polycrystalline Silicon on a 4-inch silicon wafer (Figure 1a). The patterning of the

sacrificial layer (Figure 1b) is done writing lines 2-5 μm wide and 120 μm long in the resist via photolithography and subsequent etching by RIE (reactive ion etching). All the photolithographic steps of this process have been done impressing the resist AZ1512HS with a h-line laser (405 nm) of a mask-less aligner (dose between 40 - 60 mJ/cm^2). Due to the small thickness of the two layers involved (50 nm of Si to be removed and 200 nm of SiO_2 not to be damaged) a low etching rate recipe has been used: C_4F_8 (55 sccm) - SF_6 (26sccm) for 22 s (power coil 1500W, power plate 15W, temperature 20°C, chamber pressure 30 mbar). It is important to note that the nanometric dimension is determined by the thickness of the sacrificial layer and not by the width of the nanochannel, thus allowing the definition of the nanochannel through common photolithography without the need of using a more complex e-beam lithography step. The Silicon sacrificial layer was then encapsulated with 200 nm of SiO_2 (Figure 1c) using the same process used for the first layer to avoid stress mismatching in the structure. Openings at the two extremities of the buried silicon layer are patterned via photolithography followed by (Figure 1d) RIE etching using CHF_3 (175 sccm)/ H_2 (30 sccm)/ C_4F_8 (10 sccm) recipe for 60 s (power coil 1200W - power plate 300W - temperature 10°C). The sacrificial layer is then removed using XeF_2. It has been noticed that a short RIE etching step with SF_6, just before the exposition to the XeF_2, helps for a faster and uniform etching in all regions of the wafer, very likely acting on the superficial layer of native oxide present on silicon. Sacrificial layer etching step required some optimization on the parameters for the pulsed XeF_2 etching, i.e. number and duration of the pulses and pressure of the chamber. The very narrow aperture of the channels, nanometric in height and some micrometers in width, requires 27-30 pulses lasting 180 s to allow the diffusion of the etchant along the nanochannels and to the complete removal of the sacrificial layer (Figure 1e). At last, the clamped-clamped beam geometry is defined through photolithography through the aperture of two openings in the oxide beside the released channel (visible in Figure 1g) via RIE etching (CHF_3 15sccm – 60 s, power and temperature as above) and released with a SF_6 (300 sccm – 45 s – power coil 2000W – Temperature 30°C – Pressure 100 mbar) isotropic etching (Figure 1f), exploiting the lateral undercut to remove the silicon underneath the beams. The silicon oxide structural layer is barely affected by the final SF_6 etching since the selectivity of this process over the silicon is 200:1 [26]. The length of the apertures defines the suspended part of the beam (50 μm), while the distance between them represents the width of the beam, which is 2 μm longer than the width of the inner channel on each side. Example of a complete released structure can be seen in Figure 1g.

2.3 Packaging

The sealing of the chip is performed by anodic bonding of a Schott Borofloat wafer, on which the microfluidic channels and the vibrational cavities were previously structured via hydrofluoridric acid (HF) wet etching with a chromium/gold (Cr/Au) hard mask patterned through photolithography. Powder blasting was used to create the through holes used as fluid inlet/outlet. The bonding process is carried out at 450°C with a voltage of 800 V. A higher voltage than the standard recipe was required due to the presence of a layer of silicon oxide on the surface of the wafer[27]. The microfluidic channels of the chip were connected to the external fluidic circuit controlled by a pressure controller through a custom 3D printed chip connector. This chip connector (shown in Figure 1j-k) was composed by two parts: a lower component to host the piezoelectric disk and the chip fabricated in Poly(methyl methacrylate) (PMMA) by milling

machining, and a top part fabricated by 3-D printing containing 4 channels for the liquid handling and an additional one for vacuum or gas connection. In terms of device fabrication yield, anodic bonding represents the limiting step, since a not complete adherence of the two wafers bring to liquid leakages between the bypass microchannels and the resonance cavity. Bad bonding results mostly from imperfection in the glass wafer induced by powder blasting which create both macroscopic and microscopic defects and does not always guarantee a perfectly flat surface. A final process fabrication yield can be estimated around 50%.

3. Characterization

The mechanical characterization was done using a MSA-500 (Micro system analyzer) from Polytec GmbH based on a laser-Doppler vibrometer (LDV) that can optically sense the displacement of the beams and a signal generator connected to a piezoelectric disc for external excitation of the device. The resonance frequency and the quality factor of the first resonance flexural mode of 15 devices have been extrapolated using a Lorentzian fit on the squared displacement spectrum of the suspended nanochannel resonator. All the measurements were performed in standard conditions for temperature and pressure (25°C, 1 atm). The comparison of the experimental values of the resonance frequency of the devices with the theoretical model of a doubly clamped beam confirmed the presence of a small tensile stress of about 12 MPa (determined both analytically and by FEM simulation), which is in line with typical values of stress induced by anodic bonding [23]. The small value of the stress placed the resonator in between beam and string regime, since both flexural rigidity and stress have to be taken into account to accurately determine the theoretical resonator frequency response [22, 28].
In order to evaluate the experimental responsivity, the resonance frequency was first detected in condition of empty nanochannel (only air), and then the mechanical response was characterized filling the nanochannel first with ethanol (density 789 kg/m^3) and then with water (density 999 kg/m^3). A typical example of the normalized resonance peaks for the 3 μm wide nanochannel is shown in Figure 2a (resonance frequency with air 1.559 MHz).

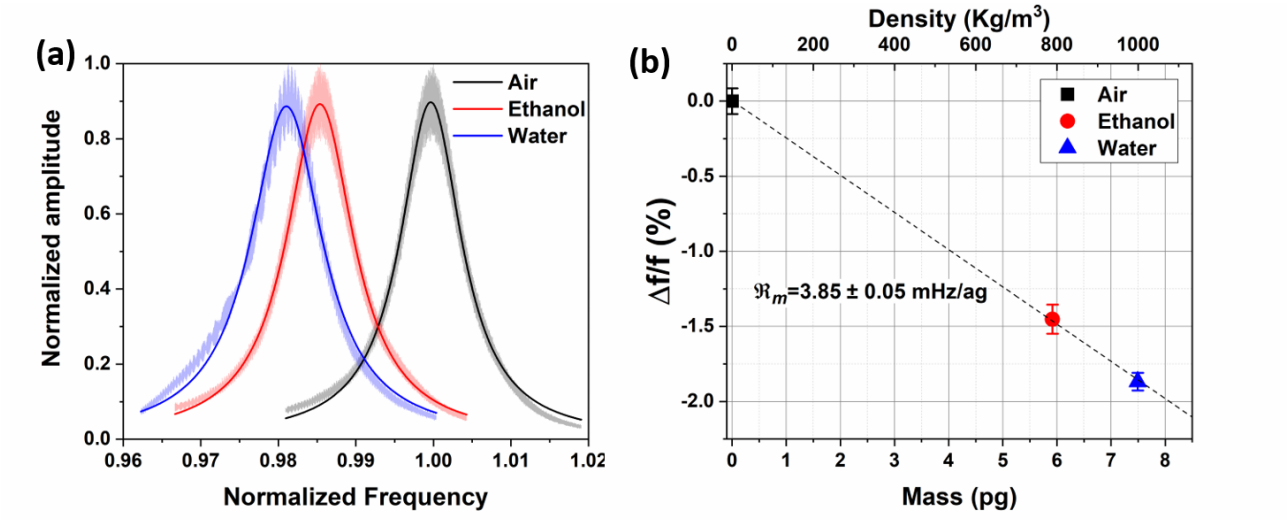

Figure 2: SNRs Characterizations. a) Resonance curves and fit of the SNR filled with different fluids: the shift increases with the fluid density (resonance frequency with air 1.559 MHz). b) Plot of the frequency shifts as a function of the mass (and density) of the liquid inside the channel for the evaluation of the SNR mass responsivity (slope of the linear fit, black dashed line).

The shifts of the resonance frequency calculated with respect to the empty case are expected to be dependent of the added mass according to equation (1). Since the geometry of the nanochannel is fixed, the mass variation of the resonator is directly related to the different fluid density. These shifts are plotted as function of the mass in Figure 2b, where errors bars come from multiple measurements made on the same devices by filling and then removing the liquid from the nanochannels. Dashed line in Figure 2b represents the fit of the experimental data according to eq (1). From the slope, it is possible to extrapolate the mass responsivity of the resonator as 3.85 ± 0.05 mHz/ag for the bridge under analysis. Results from other devices with same nominal dimensions span between 1.25 mHz/ag and 3.90 mHz/ag, which is in line with the theoretical value of 3.26 mHz/ag. The quality factor of the first flexural resonance peak was found to be mainly related to the viscous damping of air, with an average value of Q = 100 ± 10 (calculated among different devices), exhibiting no correlation with the fluid present in the channel. Variations of mass responsivity and Q factor among similar devices are ascribable to manufacturing tolerances and to a possible not complete removal of sacrificial layer, which could locally reduce nanochannel cross-section.

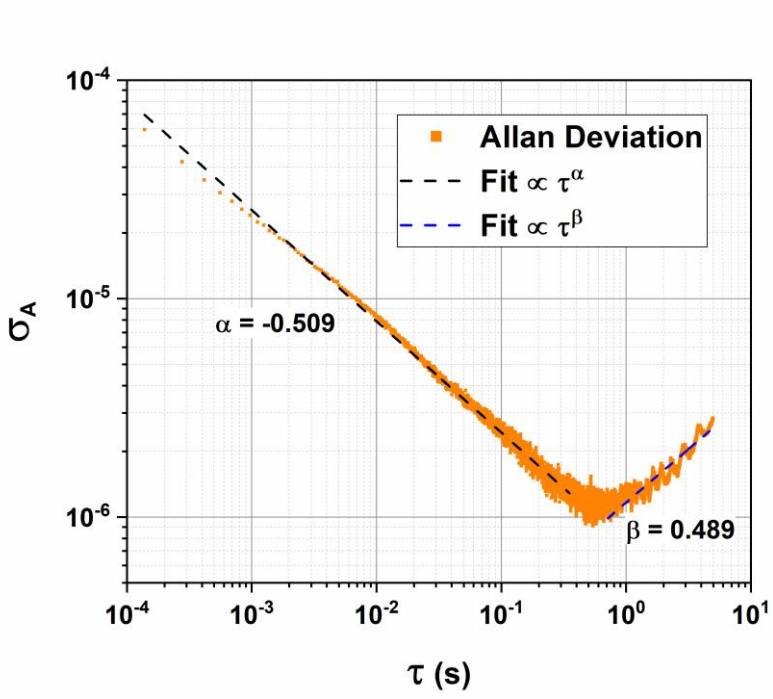

Figure 3: SNRs frequency stability. Frequency noise of the SNR, quantified as the Allan deviation normalized by the mean frequency, plotted as a function of the averaging time. The plot can be divided in a descending and an ascending part, that exhibit exponential behaviors of power ± 0.5. The dashed lines represent the fit of those two parts, with -0.509 and +0.489 as fitted exponents, giving an idea of the accuracy of the characterization.

The frequency fluctuations of the resonator has been evaluated by means of the Allan deviation measured with a lock-in amplifier (UHFLI, Zurich instruments)[29, 30]. Allan deviation was

evaluated in an open-loop configuration by measuring the response of the resonator actuated at a fixed driving frequency (the resonance frequency). The phase of the measured signal was monitored and then transformed into frequency fluctuations using the phase response of the resonator, which is linear close to the resonance frequency. The obtained results are reported in Figure 3. For low integration time (τ), a decreasing of the frequency fluctuations with a trend proportional to $\tau^{-0.5}$ is observed as the noise contribution is mainly related to thermomechanical noise (white noise). For high integration time, the noise is increasing as $\tau^{0.5}$ because of the predominant contribution of the thermal drift. Between these two regions, the lowest frequency fluctuation corresponding to 0.911 ppm is observed for integration time of 543.66 ms. Since this value represents the lower appreciable frequency shift induced by resonator mass variation, according to equation [30, 31]:

$$\frac{\partial m}{m} = 2\frac{\partial f}{f_0} = 2\sigma_a \rightarrow \partial m = 2\sigma_a * m \quad (2)$$

a minimum detectable mass of 595 ag can be estimated (σ_a represents the Allan deviation).

4. Conclusions

In this paper, a flexible and versatile process for the wafer-scale fabrication of Suspended Nanochannel Resonators (SNRs) with a yield around 50% is presented. The process is based on a sacrificial layer approach with releasing of the channel done with a xenon difluoride (XeF_2) based dry etching. The dry etching approach allows a fast removal of the dummy material with respect to the commonly used wet etching approaches. The vertical dimension (height) of the channel is defined by the thickness of the sacrificial layer, while the horizontal dimensions (length and width) are patterned through photo-lithographic steps, so that all the dimensions can be easily adjusted to the application needs and precisely tuned. For the first time in a top-down fabrication approach, the critical dimension of the channel in a SNR was reduced up to 50 nm. Fabricated devices are composed by microbeams that are 50 μm long, 7μm width and 450 nm thick, with embedded nano-channels that are 50 nm high and 3 μm width. They show a mass responsivity up to 3.90 ± 0.72 mHz/ag, estimated analyzing the shift in resonance frequency due to filling the channels with liquids of different density. The minimum detectable mass was found up to 595 ag, estimated from Allan deviation analysis. Such a fabrication process can be used as a starting point for a further scaling down of the devices embedding channels with both height and width at the nanoscale, i.e. using electron beam lithography instead of photolithography in the sacrificial layer patterning, and so pushing the mass responsivity down to the single nanoparticle or molecule resolution.

Acknowledgements

This research was partially supported by the Compagnia di San Paolo with the Project for internationalization of research and Ministero dell'Istruzione, dell'Università e della Ricerca (MIUR) through PRIN2017 - Prot.20172TZHYX grant. We thank all the CMi@EPFL staff for the support received in the fabrication part.

Author Contributions

The manuscript was written through contributions of all authors.

Notes

The authors declare no competing financial interest.

References

[1] J.L. Arlett, E.B. Myers, M.L. Roukes, Comparative advantages of mechanical biosensors, Nature Nanotechnology 6(4) (2011) 203-215

[2] I. Ferrante, N. Ciprianetti, S. Stassi, K. Santoro, S. Ferrero, L. Scaltrito, C. Ricciardi, High-Throughput Characterization of Microcantilever Resonator Arrays for Low-Concentration Detection of Small Molecules, Journal of Microelectromechanical Systems 26(1) (2017) 246-254 7786828.

[3] O. Malvar, J.J. Ruz, P.M. Kosaka, C.M. Domínguez, E. Gil-Santos, M. Calleja, J. Tamayo, Mass and stiffness spectrometry of nanoparticles and whole intact bacteria by multimode nanomechanical resonators, Nat. Commun. 7 (2016) 13452.

[4] S. Stassi, A. Chiadò, V. Cauda, G. Palmara, G. Canavese, M. Laurenti, C. Ricciardi, Functionalized ZnO nanowires for microcantilever biosensors with enhanced binding capability, Analytical and Bioanalytical Chemistry 409(10) (2017) 2615-2625

[5] P.M. Kosaka, M. Calleja, J. Tamayo, Optomechanical devices for deep plasma cancer proteomics, Seminars in Cancer Biology 52 (2018) 26-38

[6] S. Stassi, E. Fantino, R. Calmo, A. Chiappone, M. Gillono, D. Scaiola, C.F. Pirri, C. Ricciardi, A. Chiadò, I. Roppolo, Polymeric 3D Printed Functional Microcantilevers for Biosensing Applications, ACS Applied Materials and Interfaces 9(22) (2017) 19193-19201

[7] I. Roppolo, A. Chiappone, A. Angelini, S. Stassi, F. Frascella, C.F. Pirri, C. Ricciardi, E. Descrovi, 3D printable light-responsive polymers, Materials Horizons 4(3) (2017) 396-401

[8] C. Accoto, A. Qualtieri, F. Pisanello, C. Ricciardi, C.F. Pirri, M.D. Vittorio, F. Rizzi, Two-Photon Polymerization Lithography and Laser Doppler Vibrometry of a SU-8-Based Suspended Microchannel Resonator, Journal of Microelectromechanical Systems 24(4) (2015) 1038-1042 6995979.

[9] Y. Yoon, I. Chae, T. Thundat, J. Lee, Hydrogel Microelectromechanical System (MEMS) Resonators: Beyond Cost-Effective Sensing Platform, Advanced Materials Technologies 4(3) (2019) 1800597.

[10] T.P. Burg, M. Godin, S.M. Knudsen, W. Shen, G. Carlson, J.S. Foster, K. Babcock, S.R. Manalis, Weighing of biomolecules, single cells and single nanoparticles in fluid, Nature 446(7139) (2007) 1066-1069

[11] K.L. Ekinci, Y.T. Yang, M.L. Roukes, Ultimate limits to inertial mass sensing based upon nanoelectromechanical systems, J. Appl. Phys. 95(5) (2004) 2682-2689

[12] A. De Pastina, L.G. Villanueva, Suspended micro/nano channel resonators: A review, Journal of Micromechanics and Microengineering 30(4) (2020) 043001.

[13] S. Marquez, M. Álvarez, D. Fariña Santana, A. Homs-Corbera, C. Domínguez, L.M. Lechuga, Array of Microfluidic Beam Resonators for Density and Viscosity Analysis of Liquids, Journal of Microelectromechanical Systems 26(4) (2017) 749-757 7945266.

[14] W.H. Grover, A.K. Bryan, M. Diez-Silva, S. Suresh, J.M. Higgins, S.R. Manalis, Measuring single-cell density, Proceedings of the National Academy of Sciences of the United States of America 108(27) (2011) 10992-10996

[15] Y. Wang, M.M. Modena, M. Platen, I.A.T. Schaap, T.P. Burg, Label-free measurement of amyloid elongation by suspended microchannel resonators, Anal. Chem. 87(3) (2015) 1821-1828

[16] S. Olcum, N. Cermak, S.C. Wasserman, K.S. Christine, H. Atsumi, K.R. Payer, W. Shen, J. Lee, A.M. Belcher, S.N. Bhatia, S.R. Manalis, Weighing nanoparticles in solution at the attogram scale, Proceedings of the National Academy of Sciences of the United States of America 111(4) (2014) 1310-1315

[17] R.A. Barton, B. Ilic, S.S. Verbridge, B.R. Cipriany, J.M. Parpia, H.G. Craighead, Fabrication of a nanomechanical mass sensor containing a nanofluidic channel, Nano Lett. 10(6) (2010) 2058-2063

[18] A. De Pastina, D. Maillard, L.G. Villanueva, Fabrication of suspended microchannel resonators with integrated piezoelectric transduction, Microelectron. Eng. 192 (2018) 83-87

[19] M.F. Khan, S. Schmid, Z.J. Davis, S. Dohn, A. Boisen, Fabrication of resonant micro cantilevers with integrated transparent fluidic channel, Microelectron. Eng. 88(8) (2011) 2300-2303
[20] J. Kim, J. Song, K. Kim, S. Kim, N. Kim, M.F. Khan, L. Zhang, J.E. Sader, K. Park, D. Kim, T. Thundat, J. Lee, Hollow Microtube Resonators via Silicon Self-Assembly toward Subattogram Mass Sensing Applications, Nano Lett. 16(3) (2016) 1537-1545
[21] R. Calmo, A. Lovera, S. Stassi, A. Chiadò, D. Scaiola, F. Bosco, C. Ricciardi, Monolithic glass suspended microchannel resonators for enhanced mass sensing of liquids, Sensors and Actuators, B: Chemical (2019) 298-303
[22] S. Schmid, L.G. Villanueva, M.L. Roukes, Fundamentals of nanomechanical resonators, Springer International Publishing2016.
[23] M. Tilli, T. Motooka, V.M. Airaksinen, S. Franssila, M. Paulasto-Kröckel, V. Lindroos, Handbook of Silicon Based MEMS Materials and Technologies: Second Edition, 2015.
[24] F.I. Chang, R. Yeh, G. Lin, P.B. Chu, E.G. Hoffman, E.J. Kruglick, K.S. Pister, M.H. Hecht, Gas-phase silicon micromachining with xenon difluoride, Proceedings of SPIE - The International Society for Optical Engineering, 1995, pp. 117-128.
[25] S. Habermehl, A.K. Glenzinski, W.M. Halliburton, J.J. Sniegowski, Properties of low residual stress silicon oxynitrides used as a sacrificial layer, Materials Research Society Symposium - Proceedings, 2000, pp. 49-54.
[26] K.M. Eisele, Sf6, A Preferable Etchant for Plasma Etching Silicon, J. Electrochem. Soc. 128(1) (1981) 123-126
[27] T.M.H. Lee, D.H.Y. Lee, C.Y.N. Liaw, A.I.K. Lao, I.M. Hsing, Detailed characterization of anodic bonding process between glass and thin-film coated silicon substrates, Sensors and Actuators, A: Physical 86(1-2) (2000) 103-107
[28] S. Stassi, M. Marini, M. Allione, S. Lopatin, D. Marson, E. Laurini, S. Pricl, C.F. Pirri, C. Ricciardi, E. Di Fabrizio, Nanomechanical DNA resonators for sensing and structural analysis of DNA-ligand complexes, Nat. Commun. 10(1) (2019) 1690.
[29] M. Sansa, E. Sage, E.C. Bullard, M. Gély, T. Alava, E. Colinet, A.K. Naik, L.G. Villanueva, L. Duraffourg, M.L. Roukes, G. Jourdan, S. Hentz, Frequency fluctuations in silicon nanoresonators, Nature Nanotechnology 11(6) (2016) 552-558
[30] S. Stassi, G. De Laurentis, D. Chakraborty, K. Bejtka, A. Chiodoni, J.E. Sader, C. Ricciardi, Large-scale parallelization of nanomechanical mass spectrometry with weakly-coupled resonators, Nat. Commun. 10(1) (2019) 3647.
[31] A.N. Cleland, Thermomechanical noise limits on parametric sensing with nanomechanical resonators, New Journal of Physics 7 (2005) 235.